Vol. **2**, **5**. 487- 500 (2011)

**Revue de Mécanique Appliquée et Théorique**

# Optimal Control of Turbulent Channel Flow using an LES Reduced-Order Model

LAURENT CORDIER
Institut Prime, CNRS - Université de Poitiers - ENSMA. 86036 Poitiers cedex, France
Corresponding author : Laurent.Cordier@univ-poitiers.fr

ALI EL SHRIF
Department of Mechanical Engineering, Almeurgueb University, Alkhoums, Libya
Corresponding author : Laurent.Cordier@univ-poitiers.fr

**Abstract**
An optimal control approach is implemented using Large Eddy Simulations as a reduced-order model. The application of optimal control is targeting the drag reduction on the channel upper and lower walls. Three different cost functional (drag, terminal turbulent kinetic energy, mean turbulent kinetic energy) have been tested and the strategy was applied to flows going from $Re_\tau$ = 100 to $Re_\tau$ = 360. Wall transpiration (unsteady blowing/suction) with zero net mass flux is used as control. At $Re_\tau$ = 100, control managed to fully relaminarize the flow (drag reduction of about 57 %) by considering as cost functional the terminal kinetic energy. For this same cost functional, an important drag reduction of about 50 % is still obtained at $Re_\tau$ = 180 but without reaching the relaminarization. Our results show that to minimize the flow drag, it is more efficient to consider the kinetic energy as cost functional than directly the drag. Lastly, it is essential for the convergence of the minimization that the optimality system is solved on a sufficiently long time horizon.

**Résumé**
Des Simulations aux Grandes Echelles sont utilisées comme modèle réduit d'écoulement dans une approche de type contrôle optimal. L'objectif visé est de réduire la traînée de frottement sur les parois supérieure et inférieure d'un canal. Trois fonctionnelles coût différentes (traînée, énergie cinétique au temps terminal, énergie cinétique moyen) ont été testées et la stratégie de contrôle a été appliquée pour des écoulements variant de $Re_\tau$ = 100 à $Re_\tau$ = 360. Le contrôle est réalisé par soufflage/aspiration aux parois à débit masse nul. Pour $Re_\tau$ = 100, le contrôle est parvenu à relaminariser complètement l'écoulement (réduction de traînée de l'ordre de 57 %) en prenant comme fonctionnelle coût l'énergie cinétique au temps terminal. Pour cette même fonctionnelle coût, une réduction importante de traînée de l'ordre de 50 % est encore obtenue à $Re_\tau$ = 180 mais sans atteindre la relaminarisation. Nos résultats confirment que pour minimiser la traînée de l'écoulement, il est plus efficace de considérer comme objectif l'énergie cinétique que directement la traînée. Enfin, il est essentiel pour la convergence de la minimisation que le système optimal soit résolu sur un horizon temporel suffisamment long.

**NOMENCLATURE**

| | |
|---|---|
| $C$ | Coefficient of the Smagorinsky model |
| $(\mathcal{C}(\Phi))(t)$ | Instantaneous control cost |
| $\mathbb{D}(t)$ | Instantaneous total drag |
| $\boldsymbol{e}_x, \boldsymbol{e}_y, \boldsymbol{e}_z$ | Unit vectors codirectional with the $Ox, Oy, Oz$ axes |
| $\mathcal{J}$ | Cost functional |
| $\mathcal{J}_{drag}$ | Contribution of the drag to the cost functional $\mathcal{J}$ |
| $\mathcal{J}_{TKE(reg)}$ | Contribution of the regularized TKE to the cost functional $\mathcal{J}$ |
| $\mathcal{J}_{TKE(ter)}$ | Contribution of the terminal TKE to the cost functional $\mathcal{J}$ |
| $\ell$ | Penalty coefficient of the cost of the control in $\mathcal{J}$ |
| $\ell_{drag}$ | Penalty coefficient of $\mathcal{J}_{drag}$ in $\mathcal{J}$ ($\ell_{drag} = 0$ *or* 1) |
| $\ell_{reg}$ | Penalty coefficient of $\mathcal{J}_{TKE(reg)}$ in $\mathcal{J}$ ($\ell_{reg} = 0$ *or* 1) |
| $\ell_{ter}$ | Penalty coefficient of $\mathcal{J}_{TKE(ter)}$ in $\mathcal{J}$ ($\ell_{ter} = 0$ *or* 1) |
| $L_{ref} = \delta$ | Length of reference |
| $L_x, L_y, L_z$ | Lengths in the directions $\boldsymbol{e}_x, \boldsymbol{e}_y, \boldsymbol{e}_z$ *of the spatial domain* $\Omega$ |
| $\boldsymbol{n}$ | External normal vector |
| $n_1, n_2, n_3$ | Components in the Cartesian coordinates of $\boldsymbol{n}$ |
| $N_x, N_y, N_z$ | Number of points in the directions $\boldsymbol{e}_x, \boldsymbol{e}_y, \boldsymbol{e}_z$ *of the spatial mesh* |
| $P$ | Pressure |
| $Re_b$ | Reynolds number based on the bulk velocity |
| $Re_c$ | Reynolds number based on the centerline velocity |
| $Re_\tau$ | Reynolds number based on the reference variables |
| $S, S_{ij}$ | Strain-rate tensor |
| $t$ | Time |
| $t_o$ | Time of beginning of the optimization window |
| $t^+ = \frac{tu_\tau^2}{\nu} = Re_\tau \tilde{t}$ | Time in wall units |
| $T$ | Length of the sub-interval for the instantaneous control approach |
| $T_o$ | Length of the optimization window |
| $\boldsymbol{u}$ | Velocity component |
| $u_1, u_2, u_3$ or $u, v, w$ | Components in the Cartesian coordinates of $\boldsymbol{u}$ |

| | |
|---|---|
| $u_{ref} = u_\tau$ | Velocity of reference |
| $\sqrt{\langle u_i'^2 \rangle}$ | Root mean square of velocity |
| $u^+ = \frac{u}{u_\tau} = \widetilde{u}$ | Velocity in viscous units |
| $\boldsymbol{x}$ | Position vector |
| $x_1, x_2, x_3$ or $x, y, z$ | Components in the Cartesian coordinates of $\boldsymbol{x}$ |
| $x^+ = \frac{x u_\tau}{\nu} = Re_\tau \widetilde{x}$ | Position vector in viscous units |

**Abbreviations**

| | |
|---|---|
| DNS | Direct Numerical Simulation |
| LES | Large Eddy Simulation |
| MKM99 | Moser *et al.* (1999), see [7] |
| TKE | Turbulent Kinetic Energy |

**Greek symbols**

| | |
|---|---|
| $\Gamma_2^{\pm}$ | Channel walls |
| $\delta$ | Half width of the channel |
| $\bar{\Delta}$ | LES grid-filter width |
| $\hat{\Delta}$ | LES test-filter width |
| $\Delta t$ | Time-step |
| $\Delta_x, \Delta_y, \Delta_z$ | Mesh spacing in the directions $\boldsymbol{e}_x$, $\boldsymbol{e}_y$, $\boldsymbol{e}_z$ |
| $\Delta_{y_w}$ | Minimal mesh spacing in $\boldsymbol{e}_y$ |
| $\mu$ | Dynamic viscosity coefficient |
| $\nu = \frac{\mu}{\rho}$ | Kinematic viscosity coefficient |
| $\nu_T$ | Total eddy viscosity, sum of the physical viscosity and turbulent eddy viscosity. |
| $\rho$ | Density |
| $\tau_{ij}$ | Stress tensor |
| $\tau_w$ | Average stress on walls |
| $\Phi$ | Control parameter: suction and blowing on $\Gamma_2^{\pm}$ |
| $\Omega$ | Spatial domain |

**Superscripts and operators**

$(\cdot)'$ Fluctuating quantity

$(\cdot)^+$ Variables in wall coordinate or wall units

$(\cdot)^*$ Adjoint variables

$\overline{(\cdot)}$ LES grid-filtered variables

$\widetilde{(\cdot)}$ LES test-filtered variables

$\widetilde{(\cdot)}$ Variables non dimensionalized by $u_{ref}$ and $L_{ref}$

$\langle\cdot\rangle_{XZ}$ Average operator in the statistical homogeneous directions $e_x$ and $e_z$

## 1. INTRODUCTION

Optimizing internal and external aerodynamics of an aircraft with flow control has always been considered as a major issue in the development of aeronautics. Indeed, since much of the energy expended during a flight is invested to overcome the drag force exerted by the air on the aircraft body (wings, fuselages, drifts), reducing this force using flow control would increase the flight autonomy, or even decrease the takeoff weight, which would have for consequence to reduce consequently the operational costs.

From a general prospect, flow control can always be viewed as an optimization process for which an appropriate cost functional is minimized under the constraints of the flow state equations, generally considered as the Navier-Stokes equations. In this context, optimal control theory [5] seems well adapted to the resolution of this type of problems. The optimal control parameters are then searched as the solution of the so-called optimality system (coupled system of partial differential equations formed by the state equations, adjoint equations and optimality conditions), associated to the constrained optimization problem. For

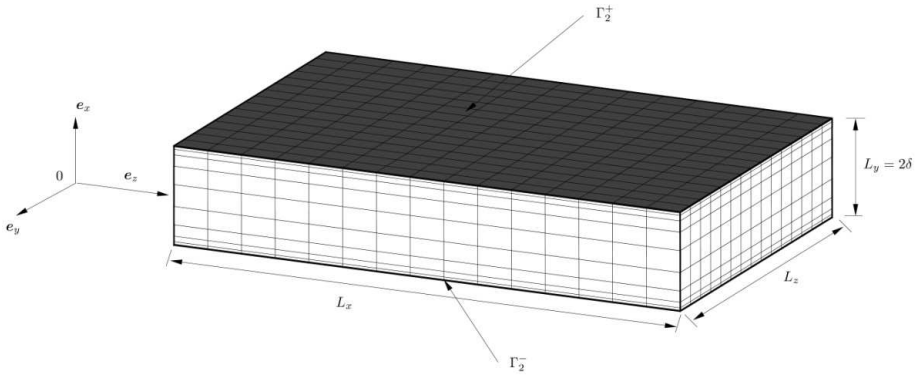


**Figure 1:** Computational domain and system of coordinates.

a three-dimensional turbulent flow, the computational costs for solving the optimality system are so high that an iterative procedure must be used (see the description in section 4). These difficulties can

be partly overcame by replacing in some phases of the optimization process, the high-fidelity model of the flow obtained traditionally by Direct Numerical Simulation (DNS) by an appropriate approximate model which can represent the essential characteristics of the flow dynamics. In this paper, we have implemented optimal control of a turbulent channel flow (see Fig. 1) using Large Eddy Simulations (LES) as an approximate model. Compared to DNS, the computational costs are greatly reduced, allowing the application of optimal control scheme to flows at higher Reynolds numbers. However, the reduction of cost offered by LES is not sufficient to optimize a three-dimensional turbulent flow over a large time horizon $T_o$. In practice, we have used the *receding-horizon predictive control* [see 4 for the details]. Briefly, this method consists of dividing the optimization time horizon $T_o$ into short sub-intervals of length T and to solve the optimal control problem in each time window using as initial conditions the control obtained in the previous time window. The procedure is repeated until the end of the total time horizon considered (see Fig. 2). However, so far, there is no evidence that the optimal control obtained using this algorithm corresponds to that which would have been obtained if one had applied the iterative procedure directly over the full time horizon $T_o$.

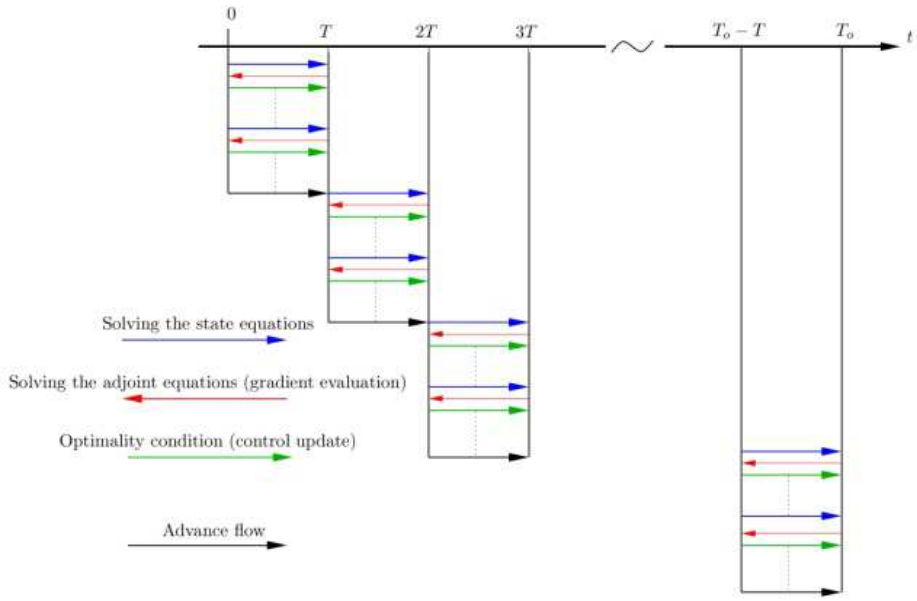


**Figure 2 :** Instantaneous control approach.

The paper is organized as follows: in section 2, a brief description of the numerical methods used to solve the LES model is first given. Then, in section 3, numerical results obtained for the case of the uncontrolled flow are presented to validate the LES code. In the next section, optimal control theory is applied targeting the reduction of the drag force on the upper and lower walls of the turbulent channel flow. Results of optimal control for flows at different Reynolds numbers and a detailed analysis for the resulting controlled flow dynamics are then presented (section 5). Finally, we give some concluding remarks and suggestions for future development.

## 2. NUMERICAL METHODS

In this study, a Smagorinsky model with a dynamic procedure suggested by [6] is used for the LES model. The coordinates and velocities are normalized by the channel half width $\delta$ and the friction velocity $u_\tau = (\tau_w/\rho)^{1/2}$, where $\tau_w$ is the averaged wall shear stress and $\rho$ is the density. All results for controlled and uncontrolled flow are presented in viscous units, with $t^+ = tu_\tau^2/\nu$, $y^+ = yu_\tau/\nu$ and $u^+ = \frac{u}{u_\tau}$. The flow is assumed periodic in the streamwise $e_x$ and spanwise $e_z$ directions. The computational grid is uniform in these two homogeneous directions and stretched using tangent hyperbolic function in the wall-normal direction. The dimensionless filtered momentum equations (see equation 2) are solved with classical numerical methods described in [4]. Finally, all simulations are carried out with a constant mass flow.

## 3. LES VERSUS DNS FOR UNCONTROLLED FLOW

In the case of uncontrolled channel flow at $Re_\tau$ = 180, the LES code is first validated by comparing for two different grid resolutions, the resulting statistics with those obtained in the reference DNS of [7] (thereafter noted as MKM 99). Table 1 gives all the parameters involved in our simulations with the corresponding Reynolds number. The channel lengths are indicated as $L_x$, $L_y$ and $L_z$, the corresponding grid points are given as $N_x$, $N_y$ and $N_z$, and finally the resolutions are given in wall units as $\Delta_x^+$, $\Delta_{y_w}^+$ and $\Delta_z^+$. The size of the computational domain in the streamwise and spanwise directions were adjusted so that the velocity fluctuations are uncorrelated before the channel center was reached. For clarity issues, the table gives also the corresponding Reynolds numbers based on the mean bulk velocity $Re_b$ and that based on the center line velocity $Re_c$. The mean velocity profiles of our DNS ($S_1$) and LES ($S_2$) simulations are compared in Fig. 3(a) against the corresponding profile obtained in MKM 99. The resulting LES mean velocity profile is in good agreement with the DNS in the near wall region, and also in the buffer zone. However, some discrepancies appeared in the logarithmic region for $S_1$. In addition, the root mean squares (rms) of velocity fluctuations in the streamwise, wall-normal and spanwise directions are compared with those of MKM 99 in Figs. 3(b), 3(c) and 3(d) respectively. The streamwise component is slightly over-estimated, while spanwise and normal components are slightly under-predicted. As for the mean velocity profile, $S_2$ outperforms $S_1$ to predict the variations of the rms profiles with a reasonable numerical costs. The resulting accuracy of these first and second order statistics demonstrates that $S_2$ can be used as a successful candidate to produce turbulent flow dynamics close to that obtained by DNS.

**Table 1:** Simulation parameters for the uncontrolled flow.

| | $Re_\tau$ | $Re_b$ | $Re_c$ | $L_x$ | $L_y$ | $L_z$ | $N_x$ | $N_y$ | $N_z$ | $\Delta_x^+$ | $\Delta_{y_w}^+$ | $\Delta_z^+$ | $\Delta t^+$ |
|---|---|---|---|---|---|---|---|---|---|---|---|---|---|
| $S_1$(DNS) | 180 | 5610.7 | 3278 | $4\pi$ | 2 | $\frac{4}{3}\pi$ | 192 | 129 | 160 | 11.8 | 0.12 | 4.7 | 0.09 |
| $S_2$(LES) | 180 | 5549.0 | 3189.4 | $4\pi$ | 2 | $\frac{4}{3}\pi$ | 64 | 73 | 96 | 35.3 | 0.22 | 7.85 | 0.36 |
| MKM 99(DNS) | 180 | – | 3300 | $4\pi$ | 2 | $\frac{4}{3}\pi$ | 128 | 129 | 128 | 17.5 | 0.05 | 5.8 | – |

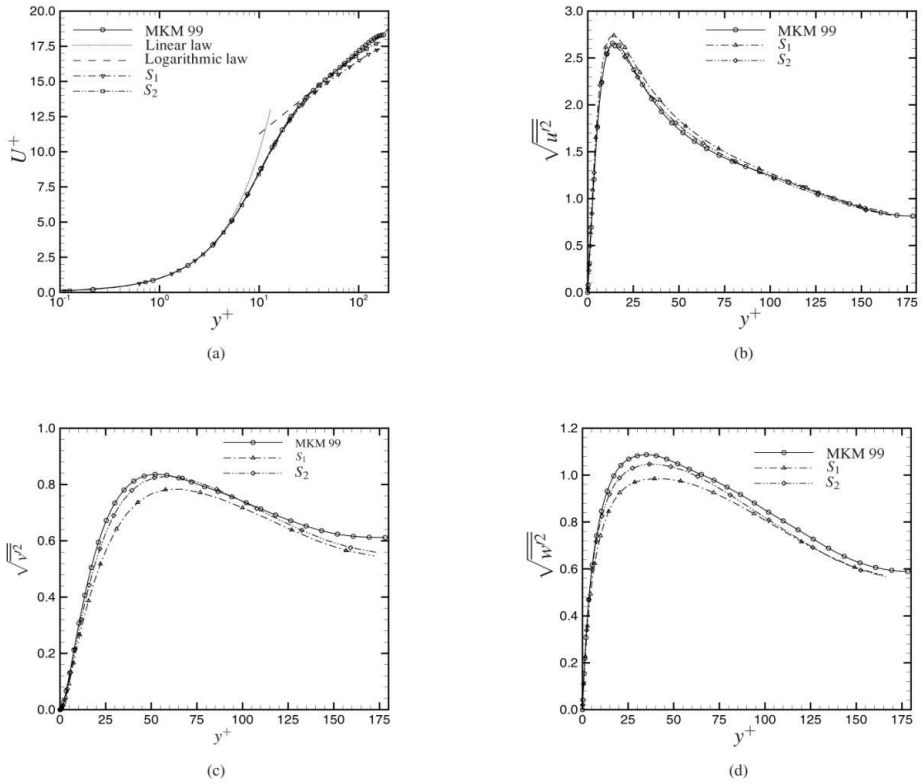


**Figure 3:** Comparisons of the first and second order statistics obtained by LES at $Re_\tau$ = 180 to the DNS results of [7]. (a) Mean velocity profile. (b), (c) and (d) Profiles of rms velocity fluctuations in streamwise, wall-normal and spanwise directions.

## 4. OPTIMAL CONTROL USING LES

The basic idea of the optimal control approach [5,4] is to minimize a cost functional, which represents the physical quantity to be optimized. So as to make the control interesting from an economic point of view, the energy spent to implement it must be an order of magnitude less than that gained from its application. Based on this general principle, one can determine the control $\Phi$ to be applied on the upper and lower walls of the turbulent channel flow by defining a cost functional based on the physical quantity of interest and the energetic representation of the control itself. Since the turbulent kinetic energy (TKE) is responsible for increasing the momentum transport from the center of the channel to the near-wall region, the kinetic energy can be viewed as the cause of turbulence and the drag as the effect. It is then reasonable for the cost functional to target directly the cause (TKE) rather than the effect (drag). A cost functional targeting the minimization of the total kinetic energy or/and the kinetic energy at the end of a time window of length $T_o$ or/and the drag can be written as:

$$J(\bar{u},\Phi) = \frac{\ell}{2}\int_{t_0}^{t_0+T_0}\int_{\Gamma_2^+}\Phi^2\,dxdt + \frac{\ell_{reg}}{2}\int_{t_0}^{t_0+T_0}\int_{\Omega}|\bar{u}(\Phi)|^2\,dxdt$$
$$+\frac{\ell_{tar}}{2}\int_{\Omega}[\bar{u}_i(\Phi)\bar{u}_i(\Phi)]_{t=t_0+T_0}\,dx + \ell_{drag}\int_{t_0}^{t_0+T_0}\int_{\Gamma_2^+}(-\tau_{12}n_2)\,dxdt. \quad (1)$$

The quantities with overbars correspond to filtered LES variables. The first term is a measure of the magnitude of the control. This quantity is integrated over the wall sections $\Gamma_{\frac{1}{2}}^{\pm}$ and time horizon $T_o$ under consideration. $\ell$ is a regularization parameter which represents the price of the control. This parameter must be taken small if the control is considered to be cheap and large for expensive control settings. The second term ($\mathcal{J}_{TKE(reg)}$) represents the time-averaged value of the turbulent kinetic energy, while the third term ($\mathcal{J}_{TKE(ter)}$) targets the terminal value of the kinetic energy *i.e.* the value at the end of each optimization horizon. Finally, the last term ($\mathcal{J}_{drag}$) is a measure of the drag. Using optimal control theory, this problem can be cast as an optimization process where the cost functional (1) can be minimized under the constraint of the state equations represented by the LES momentum equations *i.e.*

$$\mathcal{L}_i(\bar{u},\bar{P}) = \frac{\partial \bar{u}_i}{\partial t} + \frac{\partial}{\partial x_j}(\bar{u}_i\bar{u}_j) - 2\frac{\partial}{\partial x_j}(\nu_T \bar{S}_{ij}) + \frac{\partial \bar{P}}{\partial x_i} = 0, \tag{2}$$

where $\bar{S}_{ij} = \frac{1}{2}\left(\frac{\partial \bar{u}_i}{\partial x_j} + \frac{\partial \bar{u}_j}{\partial x_i}\right)$ represents the strain-rate tensor of the filtered velocity field. These state equations are subjected to suitable initial and boundary conditions. In particular, the control $\Phi$, which corresponds to suction and blowing on the walls, intervenes via the boundary condition $\bar{u}_2|_{\Gamma_{\frac{1}{2}}^{\pm}} = -\Phi n_2$ where $n_2$ is the outward unit vector. Here, $\nu_T$ is the nondimensional total viscosity, defined as $\nu_T = 1/Re_\tau + C\bar{\Delta}^2|\bar{S}|$ where $C$ is the Smagorinsky dynamic constant, $\bar{\Delta}$ is the grid-filter width and $|\bar{S}| = \left(2\bar{S}_{ij}\bar{S}_{ij}\right)^{1/2}$. After introduction of the adjoint variables $\bar{u}_i^*$ and $\bar{P}^*$, the Lagrange multipliers technique can be used to transform the original constrained optimization problem to an unconstrained optimization problem. The variation of the cost functional (1) with respect to the state variables gives the adjoint equations which are found to be [4]:

$$\begin{aligned}\mathcal{L}_i{}^*(\bar{u}^*,\bar{P}^*) = &-\frac{\partial \bar{u}_i^*}{\partial t} - 2\bar{u}_j\bar{S}_{ij}^* + \frac{\partial \bar{P}^*}{\partial x_i} - 2\nu\frac{\partial \bar{S}_{ij}^*}{\partial x_j} \\ &-\frac{\partial}{\partial x_j}\left(\frac{4C\bar{\Delta}^2}{|\bar{S}|}\bar{S}_{kl}\bar{S}_{kl}^*\bar{S}_{ij}\right) - \frac{\partial E_{ij}}{\partial x_j} - B_i - \ell_{reg}\bar{u}_i = 0.\end{aligned} \tag{3}$$

These equations are subjected to the following boundary and terminal conditions:

$$\bar{u}_i^*|_{\Gamma_{\frac{1}{2}}^{\pm}} = 0 \quad i = 1,2,3 \ \ (BC) \qquad and$$

$$\bar{u}_i^*(t_0 + T_o) = \bar{u}_i\ (t_0 + T_o)\ \ i = 1,2,3\ \ (TC).$$

The expressions of the tensors $E_{ij}$ and $B_i$ are very complex. They are given (see Appendix) as a function of the resolved states and adjoint fields. These terms arise from the variation of the dynamic

model constant $C$ with respect to the state variables [4]. Finally, the variation of (1) with respect to the control variables provides the optimality conditions given by:

$$\frac{\mathcal{D}\mathcal{J}}{\mathcal{D}\Phi} = \ell\Phi + E_{22} - \bar{P}^{*}. \tag{4}$$

Equations (2), (3) and (4) form what is called the optimality system. This system of coupled partial differential equations can be solved iteratively in order to find the instantaneous control parameters $\Phi$ that minimize (1) and consequently reduce the drag force on the channel walls. The control is updated using a conjugate gradient algorithm. The receding-horizon predictive control has been used for the resolution of the optimality system with sub-intervals of length $T^{+}$ going from 1.5 to 80. The corresponding algorithm is described in Fig. 4.

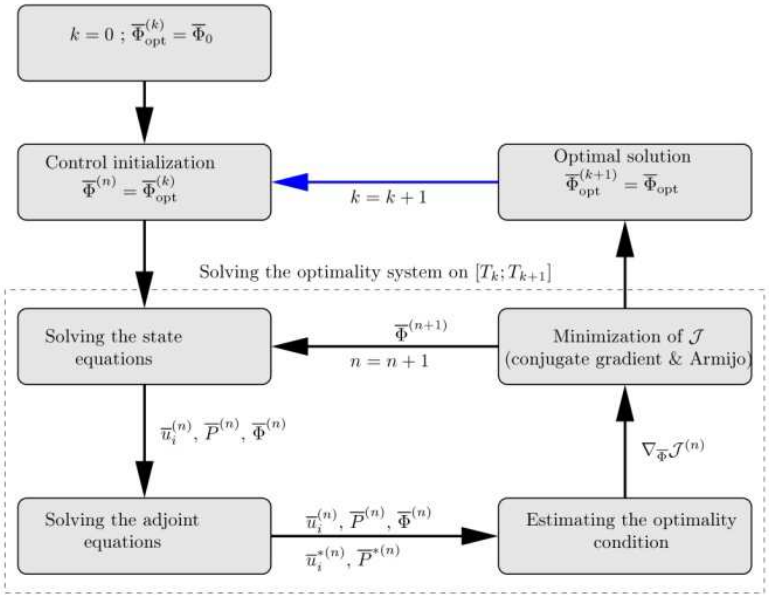


**Figure 4 :** Iterative resolution of the optimality system for a receding-horizon predictive control approach.

## 5. OPTIMAL CONTROL RESULTS

In this section, we present results of optimal control obtained using three different values of Reynolds number. We have started with $Re_\tau$ = 100 which is small enough to allow the realization of numerous control simulations at a reasonable numerical cost. A detailed analysis of the effect of some parameters involved in the optimization process has been achieved at this Reynolds number. The influence of the choice of the cost functional as well as the length of the optimization time windows have been discussed based on the results obtained. The two other values of Reynolds number that were considered, 180 and 360, correspond to super-critical turbulent flow regimes. These values were used to study the effect of an increase of the Reynolds number on the control. The parameters used to perform the optimal control simulations for the three Reynolds numbers considered are given in Table 2.

**Table 2:** Parameters used for the different optimal control simulations.

| $Re_\tau$ | $Re_c$ | $Re_b$ | $L_x$ | $L_y$ | $L_z$ | $N_x$ | $N_y$ | $N_z$ | $\Delta x^+$ | $\Delta y_w^+$ | $\Delta z^+$ | $\Delta t^+$ |
|---|---|---|---|---|---|---|---|---|---|---|---|---|
| 100 | 1817 | 3030.3 | $4\ \pi$ | 2 | $\frac{4}{3}\pi$ | 48 | 49 | 48 | 26.2 | 0.19 | 8.7 | 0.3 |
| 180 | 3214.1 | 5600.2 | $4\ \pi$ | 2 | $\frac{4}{3}\pi$ | 64 | 65 | 64 | 35.3 | 0.25 | 11.7 | 0.36 |
| 360 | 6834.2 | 12115.9 | $2\ \pi$ | 2 | $\frac{3}{4}\pi$ | 64 | 97 | 64 | 35.3 | 0.326 | 13.25 | 0.72 |

### 5.1 Influence of the choice of the cost functional

The performance of the optimal control in terms of drag reduction is very sensitive to the choice of the cost functional. Figure 5 represents the temporal evolution of the total mean drag $\mathbb{D}$ from controlled simulations performed at $Re_\tau$ = 100 for three different types of cost functional. These results clearly show that the optimization problem depends strongly on the choice of the cost functional. In terms of drag reduction, the most effective form of the cost functional corresponds to the terminal kinetic energy, where the drag is reduced by about 57 % and the flow is fully laminarized. For the two other cost functionals, drag reductions were lower. Indeed, we obtain about 37 % of drag reduction for the cost functional based on the total kinetic energy and 25 % for the cost functional that directly targets the drag on the upper and lower walls. This behavior can be explained in two ways, firstly it seems related to the physics of turbulence where the turbulent kinetic energy can be considered as the "cause" of turbulence and the drag as the "effect". In this sense, minimizing the turbulent kinetic energy has a direct effect on the drag reduction. Thus optimal control formulation based on the minimization of the turbulent kinetic energy, and more particularly the terminal kinetic energy, is more effective in reducing the drag than if a cost functional targeting directly the drag force was considered. In Fig. 6, we observe that the control cost corresponding to the minimizations of $\mathcal{J}_{TKE(reg)}$ and $\mathcal{J}_{drag}$ is equal to zero at the end of each optimization window. This behavior is due to the terminal condition of the adjoint equation which is zero in both cases. As a consequence, when the minimization of the terminal kinetic energy is the objective, the control acts uniformly throughout the optimization window. This is the second point that can explain why the formulation based on the terminal kinetic energy is more effective in terms of drag reduction. Figure 7 represents the temporal evolution of total kinetic energy for the different cost functional considered. The change in kinetic energy clearly reflects the sub-critical behavior of the channel flow at $Re_\tau$ = 100. Indeed, we find that if the control succeeds in reducing the kinetic energy below a given critical value then the flow is relaminarized. On the contrary, if this critical value is not reached as this is the case with formulations based on the kinetic energy and on the drag, there is a saturation or an increase in the kinetic energy. At $T^+$=25.5, the critical value is reached beyond $t^+ \simeq 800$ (Figs. 5 and 7). For larger values of the optimization time window $T^+$, this phenomenon happens earlier.

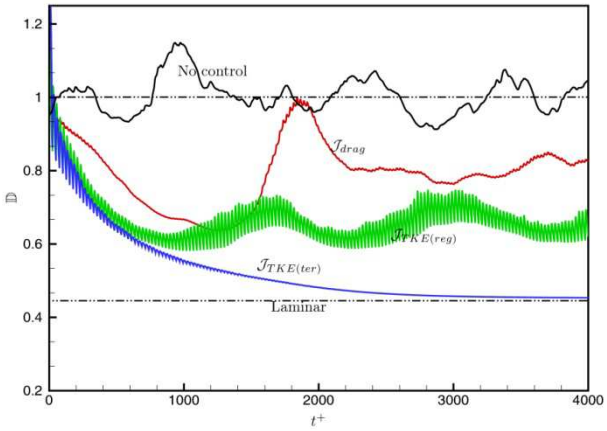


**Figure 5:** Drag history of optimal controlled flows at $Re_\tau$ =100. Three different kinds of cost functional are considered for $T^+$=25.5.

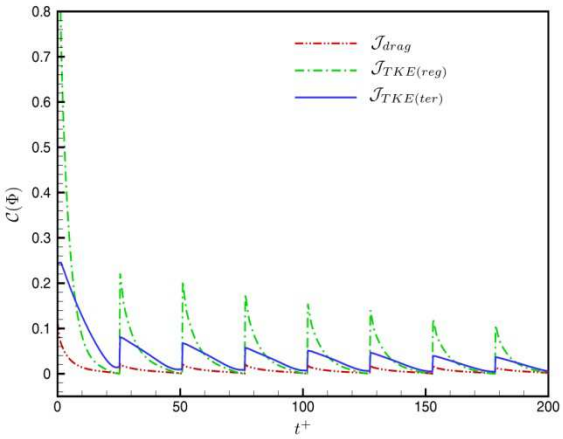


**Figure 6:** Control cost history of optimal controlled flows at $Re_\tau$ =100. Three different kinds of cost functional are considered for $T^+$ =25.5.

## 5.2 Influence of the length of the optimization time window

In the previous section, we showed that the most effective choice of cost functional in terms of drag reduction is the terminal kinetic energy formulation based on the minimization of $\mathcal{J}_{TKE(ter)}$. Here, we consider this cost functional and examine the influence of the length of the optimization time window on the convergence of the optimization procedure. Figures 8 and 9 represent, for different values of the optimization time window $T^+$ ranging from 1.5 to 80, the temporal evolution of the averaged total drag and of the total kinetic energy, respectively. These figures show that for $T^+ \geq 25.5$, the flow is laminarized: the drag tends towards the laminar value beyond $t^+ \simeq 2000$ and the total kinetic energy decreases sharply, tending to zero as the optimization time proceeds. We can see also on these figures that, as the length of the optimization time window increases, the drag and the total kinetic energy reduce rapidly. In Fig. 9, an abrupt increase of the total kinetic energy is observed beyond $t^+ \simeq 700$ for $T^+ \leq 10.5$. This increase clearly indicates the difference in behaviour at long times between the simulations carried out for $T^+ \geq 25.5$ (laminarization) and for $T^+ < 25.5$ (saturation of the kinetic energy). A probable explanation is that, at this time, occurs in the production cycle of turbulence an event of intense turbulent activity accompanied by a sudden increase in kinetic energy inside the flow. When the length of the optimization time window is large enough, the turbulent events that generate these sudden increases of the kinetic energy can be captured by the optimization process and thus be taken into account in the gradient of the cost functional. For $t^+ \simeq 700$, two antagonistic mechanisms opposed. On the one hand, there is a sudden increase in kinetic energy and, on the other hand, more drag reduction occurs. The final behavior of the system is directly related to the physical mechanism that is able to impose upon the other.

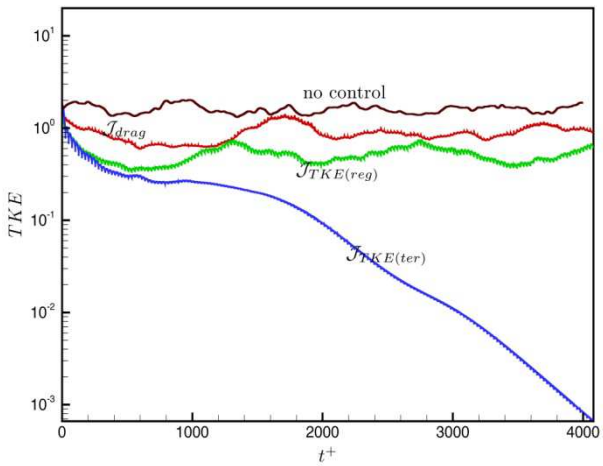


**Figure 7:** Total kinetic energy history (log scale) of optimal controlled flows at $Re_\tau$ =100. Three different kinds of cost functional are considered for $T^+$=25.5.

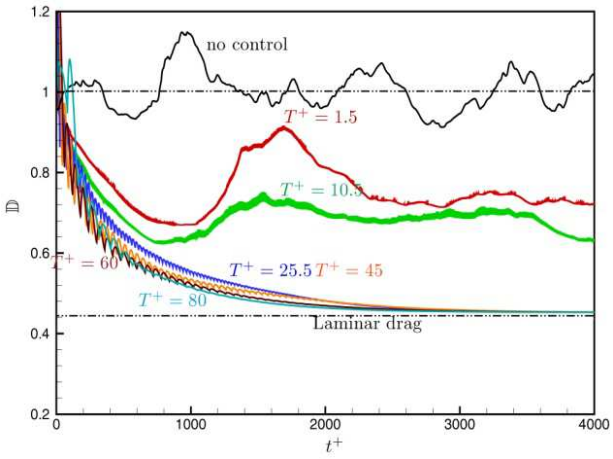


**Figure 8:** Drag history of optimal controlled flows at $Re_\tau$ =100 for the minimization of $\mathcal{J}_{TKE(ter)}$. Different optimization time windows $T^+$are considered.

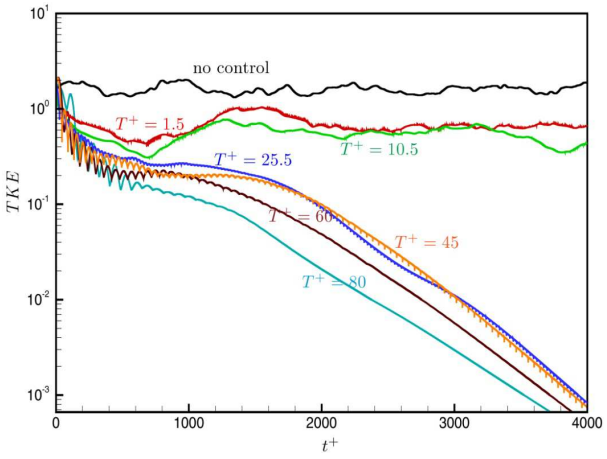


**Figure 9:** Total kinetic energy history (log scale) of optimal controlled flows at $Re_\tau$ =100 for the minimization of $\mathcal{J}_{TKE(ter)}$. Different value of $T^+$are considered.

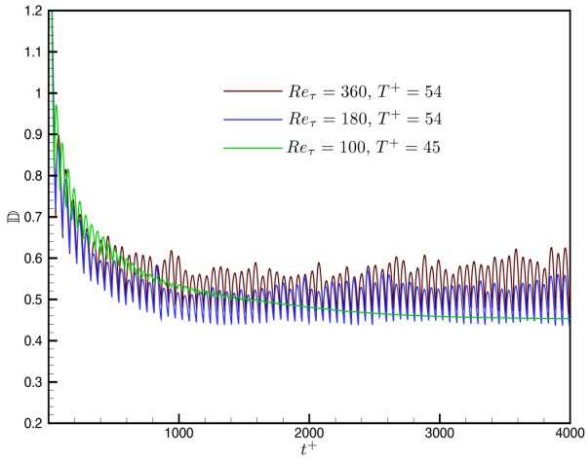


**Figure 10:** Drag history of optimal controlled flows at three Reynolds numbers ranging from 100 to 360 using $\mathcal{J}_{TKE(ter)}$ as cost functional.

### 5.3 Effect of increasing the Reynolds number

The drag histories obtained by optimal control at three values of Reynolds number ranging from 100 to 360 are compared in Fig. 10. The amount of drag reduction is of about 50 % in the case of $Re_\tau$ = 180 and of about 45 % at $Re_\tau$ = 360, which is less than the drag reduction resulting from control simulations at $Re_\tau$ = 100 (57 %). This decrease of drag reduction with the increase of the Reynolds number was already observed in the classical opposition control procedure [4]. Since turbulent events at high Reynolds number are very violent and very fast, they are hardly captured in the gradient of the cost functional. This loss of information gives incorrect gradient and contributes to an ill evaluation of control parameters, so the computed control does not match the real dynamics of the involving turbulent events.

## 6. CONCLUSION

In this work, we have used Large Eddy Simulations as a reduced-order model permitting the implementation of optimal control procedures to reduce the drag in a fully developed turbulent channel flow. Control laws were imposed as an unsteady blowing/suction on the channel walls for turbulent flows going from $Re_\tau$ = 100 to $Re_\tau$ = 360. Using LES as an approximate model led to a significant reduction in the computational costs (CPU and memory). At $Re_\tau$ = 180, we have then solved the optimality system using optimization windows much larger than that enabled by the DNS [3]. Moreover, it gave us the opportunity to perform optimal control at higher Reynolds number concluding that, at $Re_\tau$ = 360, about 45 % of drag reduction was still achieved. Our results confirm that it is more efficient to target the source of turbulence (kinetic energy) rather than its effects (drag on the walls). Indeed, we obtain that the reduction of drag is more important when the cost functional is based on the terminal kinetic energy rather than on drag. Note also that in our simulations of optimal control, the minimum drag that we have obtained corresponds exactly to the value in the laminar regime. This result seems to confirm the conjecture hypothesis advanced by [2] who claims that the minimal drag that can be achieved by a control procedure applied to a turbulent channel flow using a blowing/suction corresponds to that of the laminar flow. Unlike the case of sub-critical turbulent flow ($Re_\tau$ = 100), the optimal control procedure did not allow relaminarization of the flow at $Re_\tau$ = 180 and $Re_\tau$ = 360. Finally, a future prospect of this work is to use reduced-order models based on Proper Orthogonal Decomposition (POD). Indeed, it was recently demonstrated in [1] that it was possible to use a POD model for minimizing the drag coefficient of a cylinder wake.

## 7. ACKNOWLEDGEMENTS

This work has received support from the National Agency for Research on reference ANR- 08-BLAN-0115-01.

## 8. REFERENCES

[1] M. Bergmann and L. Cordier, “Optimal control of the cylinder wake in the laminar regime by trust-region methods and POD reduced-order models,” *Journal of Computational Physics*, vol. 227, no. 16, pp. 7813-7840, 2008.

[2] T. R. Bewley and O. M. Aamo, “A "winwin" mechanism for low-drag transients in controlled two-dimensional channel flow and its implications for sustained drag reduction,” *J. Fluid Mech.*, vol. 499, pp. 183-196, 2004.

[3] T. R. Bewley, P. Moin and R. Temam, “DNS-based predictive control of turbulence: an optimal benchmark for feedback algorithms,” *J. Fluid Mech.*, vol. 447, pp. 179-225, 2001.

[4] A. El Shrif, “Contrôle optimal d'un écoulement de canal turbulent,” *PhD thesis*, Institut National Polytechnique de Lorraine, 2008.

[5] M. D. Gunzburger, “Introduction into mathematical aspects of flow control and optimization,” *Lecture series 1997-05 on inverse design and optimization method*, Von Karman Institute for Fluid Dynamics, 1997.

[6] D. Lilly, “A proposed modification of the Germano subgrid-scale closure method,” *Phys. Fluids A*, vol. 4, pp. 633-635, 1992.

[7] R. D. Moser, J. Kim and N. N. Mansour, “Direct numerical simulation of turbulent channel flow up to $Re_\tau$ = 590,” *Phys. Fluids*, vol. 11, no. 4, pp. 943-945, 1999.

**APPENDIX. Expressions of $E_{ij}$ and $B_i$**

The tensors $E_{ij}$ and $B_i$ introduced in (3) are defined as (see [4] for the details)

$$E_{ij} = 4\left(\widehat{\rho}_{ij}\,|\bar{S}| - \eta^2\,\widehat{\rho_{ij}\left|\tilde{\bar{S}}\right|}\right) + 8\left(\widehat{\rho}_{kl}\,\frac{\bar{S}_{kl}\bar{S}_{ij}}{|\bar{S}|} - \eta^2\,\widehat{\rho_{kl}\frac{\tilde{\bar{S}}_{ij}\tilde{\bar{S}}_{kl}}{\left|\tilde{\bar{S}}\right|}}\right)$$

where $\eta = \widehat{\Delta}/\Delta$ and
$B_i = 4\left(\widehat{N_{ij}\tilde{\bar{u}}_j} - \widehat{N}_{ij}\bar{u}_j\right)$.

The tensors $P_{ij}$and $N_{ij}$ appearing in the definitions of $E_{ij}$ and $B_i$ are given respectively by

$$P_{ij} = \frac{\langle|\bar{S}|\,\bar{S}_{mn}\,\bar{S}^*_{mn}\rangle_{XZ}}{\langle M_{kl}M_{kl}\rangle_{XZ}}\,\left(L_{ij} - 2C\bar{\Delta}^2\,M_{ij}\right)$$

and

$$N_{ij} = \frac{\langle|\bar{S}|\,\bar{S}_{mn}\,\bar{S}^*_{mn}\rangle_{XZ}}{\langle M_{kl}M_{kl}\rangle_{XZ}}\,M_{ij}.$$

Moreover, the Smagorinsky dynamic constant $C$ is given [6] by

$$C(y,t) = \frac{1}{\bar{\Delta}^2}\,\frac{\langle L_{ij}M_{ij}\rangle_{XZ}}{\langle M_{ij}M_{ij}\rangle_{XZ}}$$

where
$L_{ij} = \widehat{\bar{u}_i\bar{u}_j} - \hat{\bar{u}}_i\,\hat{\bar{u}}_j$

and

$$M_{ij} = 2\left(\widehat{|\bar{S}|\,\bar{S}_{ij}} - \eta^2\,\left|\tilde{\bar{S}}\right|\,\hat{\bar{S}}_{ij}\right).$$